FRACTURE BEHAVIOUR OF A SINGLE CRYSTAL NICKEL BASE SUPERALLOY SC16

M. RUMI, W. CHEN, H. FECHT and H. WEVER
Institute of Metal Research, Technical University Berlin,
D-10623 Berlin, Germany

R.P. WAHI
Hahn-Meitner-Institute Berlin GmbH,
D-14109 Berlin, Germany

ABSTRACT

The fracture behaviour of a single crystal nickel base superalloy SC16 developed for applications as blade materials in land-based gas turbines has been investigated under monotonic loading at various temperatures (ambient temperature to 1223 K) and strain rates (10^{-3} to 10^{-6} s^{-1}). The microscopic examinations revealed that under all the test conditions the crack initiation sites in the alloy are casting pores. The crack propagation both along {001} crystallographic planes perpendicular to load axis and along {111} glide planes has been found in the examined specimens with an axial orientation of <001>. The occurrence of both the crack propagation modes depended on the test conditions used. At 1223 K a strain rate-dependence of fracture strain and a corresponding change in fractographic morphologies have been observed. This effect is rationalised using a concept of dynamic recovery which leads to an increasing localisation of deformation and damage with decreasing strain rate at high temperatures.

KEYWORDS

Nickel base superalloy, single crystal, monotonic loading, high temperature, crack initiation sites and propagation paths

INTRODUCTION

Nickel base superalloys are being increasingly used in single crystal form, especially in aerospace engines, due to improved high temperature properties in comparison with conventionally cast nickel base superalloys. Extensive studies on the mechanical behaviour of single crystal superalloys have been carried out, e.g. (Ghosh *et al.*, 1990; Milligan *et al.*, 1991; Pollock *et al.*, 1992; Socrate *et al.*, 1993; Gabrisch *et al.*, 1994). Most of these studies have been primarily directed to the deformation processes and the microstructure degradation (e.g. γ' rafts formation) in the superalloys under various test conditions at elevated temperatures. The information on fracture behaviour of single crystal superalloys under monotonic loading is more limited and can be

summarised as follows: a) The crack nucleation takes place preferentially at interdendritic γ/γ' eutectic, casting pores or carbides (Walston *et al.*, 1991; Kakehi *et al.*, 1993; Fritzemeier, 1988). b) For <001>-oriented single crystal superalloys two crack propagation paths on (001) crystallographic planes perpendicular to load axis (Hashem *et al.*, 1994; Ai *et al.*, 1992) or on {111} glide planes have been observed (Duhl, 1989). Most of these studies have been performed on creep loaded specimens. The dependence of the crack nucleation and growth behaviour has not been investigated systematically.

With the advances in alloy design and casting technology it is possible to produce single crystal blades for land-based gas turbines in sizes more than 20 cm (Goldschmidt, 1994). The single crystal nickel base superalloy SC16 based on the widely used conventionally cast polycrystalline blade alloy IN738LC has been developed for such applications (Khan *et al.*, 1990). As compared to the other single crystal superalloys used in aero engines (about 6-10 wt.% Cr and 60-70 vol.% γ' precipitates), this new class of single crystal superalloy contains a higher chromium content of 16 wt.% and a lower γ' volume fraction of about 40 % in order to obtain an optimal combination of high hot corrosion resistance, good long term phase stability as well as high temperature mechanical strength. Recently, some investigations concerning the deformation behaviour of this alloy have been conducted (Gabrisch *et al.*, 1994; Gabrisch *et al.*, 1996; Mukherji et al., 1996). In this paper we present our initial results on fracture behaviour of the superalloy SC16.

EXPERIMENTAL

The chemical composition of the superalloy SC16 investigated in the present study is given in Table 1. The specimens were subjected to the following heat treatment procedure selected on the basis of a detailed study of growth kinetics of γ' phase in this alloy (Malow *et al.*, 1994):

Solution treatment: 1528 K / 3 hrs. / cooling rate >150 K / min.
Ageing treatment: a) 1373 K / 1 hr. / cooled down to 1123 K in 15 K / hr.
b) 1123 K / 24 hrs. / AC

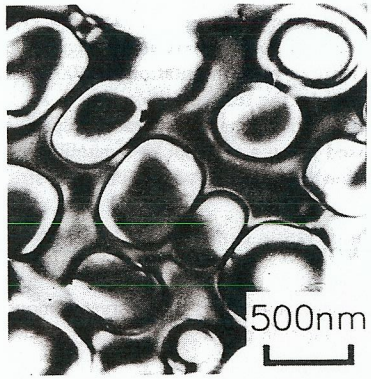

Fig. 1 Initial microstructure of SC16

After the heat treatment the specimens had a unimodal distribution of cuboidal γ' precipitates with an average edge length of 450 nm and a volume fraction of about 40 %. Figure 1 shows the initial microstructure of the alloy. The casting pores were found to be aligned along the specimen axis in interdendritic regions and had an ellipsoidal form with the long axis parallel to the specimen axis and an aspect ratio of 1.2 (Rumi *et al.*, 1994). On transverse sections of the as-received specimens a pore density of 31.6 cm^{-2} and an average pore size of 6.9 mm were measured (Rumi *et al.*, 1994).

Table 1 Chemical composition of the single crystal nickel base superalloy SC16 in wt.%

Al	C	Cr	Mo	Ta	Ti	Ni
3.46	<0.005	15.37	2.84	3.60	3.50	balance

The tensile tests were conducted on the specimens having a 9 mm gauge diameter, 12 mm gauge length and an initial axial orientation within 6° of <001>. All the tests were performed on a servohydraulic MTS testing system under constant total axial strain rates (10^{-3} - 10^{-6} s^{-1}) at various temperatures from ambient temperature to 1223 K. The strain was monitored using a clip-on high temperature extensometer. For the tests having a large fracture strain (≥ 16 %) beyond the measurement range of the extensometer the control mode of the test was switched to cross-head speed control. After the control mode change, the strain rate became slightly larger (about 4%) and remained more or less constant during further deformation.

The microporosity, crack initiation and propagation were measured or documented on fracture surfaces, and on longitudinal and transversal sections of the failed specimens using optical and Scanning Electron Microscopy (SEM).

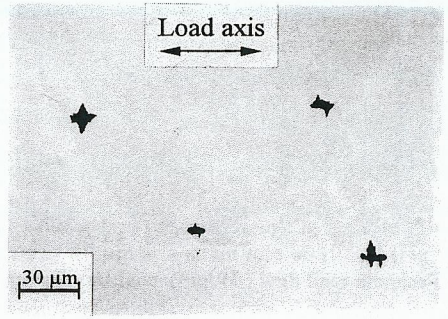

Fig. 2 Crack initiation at casting pores

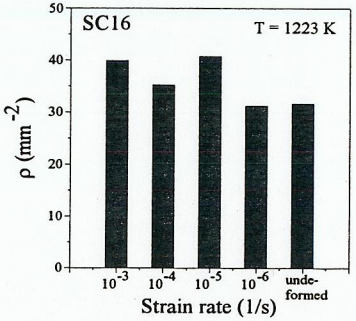

Fig. 3 Number density ρ of cracks/pores in as-received specimens and in homogeneous deformation regions at various strain rates

RESULTS AND DISCUSSIONS

Crack Initiation

The optical microscopic examinations on the as-received specimens showed that the specimens used in the present study did not contain any residual eutectic in interdendritic region, which have been found frequently to be the dominating crack initiation sites in cast nickel base superalloys (Walston et al., 1991, Fritzemeier, 1988). Under all the test conditions cracks at casting pores with crack plane approximately perpendicular to the <001> load axis were observed, see Fig. 2. The number density ρ of cracks/pores measured on transversal sections of failed specimens in homogeneous deformation zone (about 3 mm beneath fracture surface) is comparable to

that of the as-received specimen (Fig. 3). The slight increase in ρ found at higher strain rate can be attributed partly to the higher elongation of the alloy under this test condition (about 25 % at the higher strain rate) leading to i) an area reduction in transversal sections of the specimens and ii) an increase in aspect ratio of ellipsoidal casting pores. Since the total transversal section of a specimen is imaged for counting the number of pores, a reduction in the transversal section causes an increase in ρ. An increase in the aspect ratio of the pores means a higher probability of their intersecting any arbitrary cross section plane, therefore, an increase in ρ. Based on both the observations (Fig. 2 and Fig. 3) we conclude that in SC16 the cracks initiate essentially at casting pores and the deformation induced porosity is negligible.

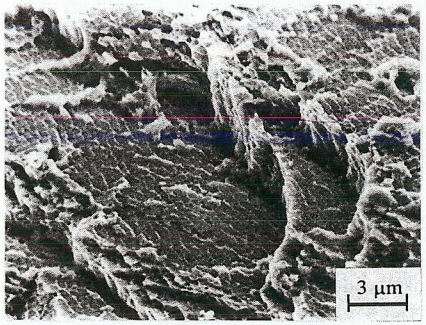

(a)

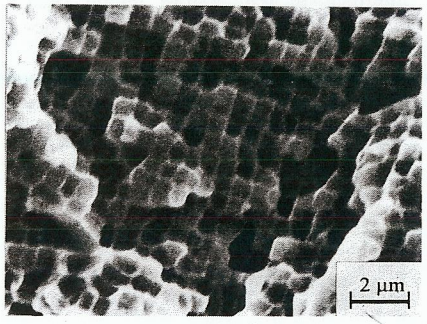

(b)

Crack propagation

Typical SEM-micrographs of tensile fracture surfaces are shown in Fig. 4a - d. Fig. 4a - c were taken in the fracture regions perpendicular to the [001]-load axis after deformation at ambient temperature, 1023 K and 1223 K, respectively. In Fig. 4b a characteristic morphology of fracture surfaces containing well recognisable γ' structure is presented. The morphology was further explored by tilting the fracture surfaces of the specimens slightly in the microscope. The γ phase surrounding the γ' precipitates appeared to be standing out against the γ' precipitates, making the latter visible (Fig. 4a). At 1223 K such γ' structure could not be observed due to oxidation of fracture surface. The dimples and particles on fracture surfaces showed, however, a similar size of about 0.5 µm as that of γ' precipitates. It is obvious that the γ' precipitates are not cleaved by cracks. Both the observations on the specimens tested at lower (ambient temperature) and higher (>1023 K) temperatures suggest that the crack propagation in SC16 proceeds along γ/γ' interphase interfaces. At the intermediate temperature of 923 K, where the maximum tensile strength was measured (Chen 1996), the crack propagation followed the {111} glide planes. The γ' precipitates exposed on fracture surfaces showed, therefore, a rough triangular geometry (Fig. 4d). The details of temperature effect on crack propagation will be reported elsewhere (Chen 1996).

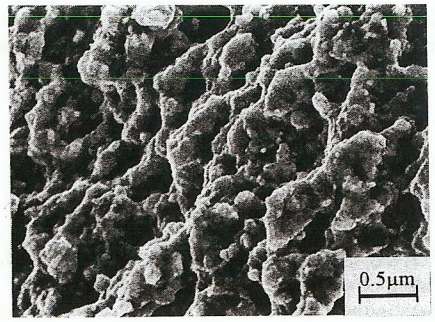

(c)

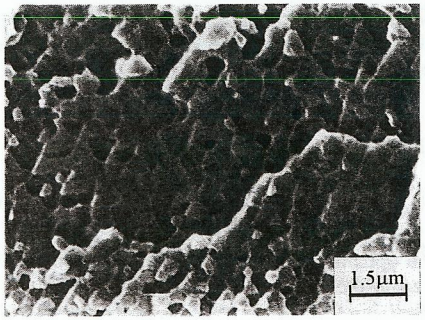

(d)

Fig. 4 Micrographs showing fractographic characteristics of specimens tested at ambient temperature (a), 1023 K (b), 1223 K (c) and 923 K (d)

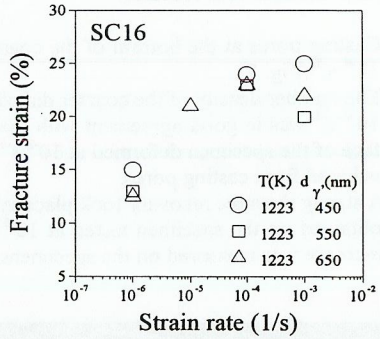

Fig. 5 Plot of fracture strain vs. strain rate

Strain rate-dependence of fracture strain and fractographic characteristics at 1223 K

At the highest temperature of 1223 K used in the present study a strain rate-dependence of fracture strain was measured (Fig. 5). The fracture strain becomes larger with increasing strain rate. A corresponding change in fractographic characteristics was detected: Coarser dimples of about 40 µm at a strain rate of 10^{-6} s^{-1} (Fig. 6a) and a macroscopically more or less "smooth" fracture surface (Fig. 6b) with finer dimples of about 0.5 µm at 10^{-3} s^{-1} (Fig. 4c) were observed.

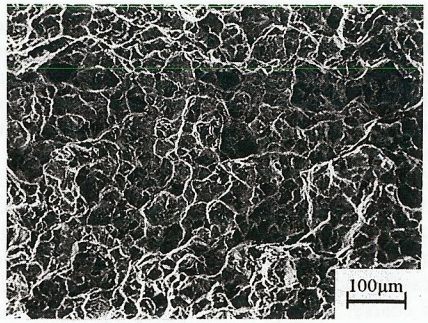

(a)

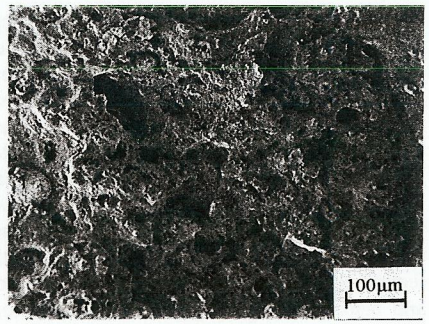

(b)

Fig. 6 SEM-micrographs showing a coarser dimple structure at 10^{-6} s^{-1} (a) and a finer ones at 10^{-3} s^{-1}

Further examinations revealed:

a) Casting pores at the bottom of the coarser dimples in the specimen tested at a strain rate of 10^{-6} s^{-1} (Fig. 7).
b) The number density of the coarser dimples (59 cm^{-2}) found in the specimen with strain rate of 10^{-6} s^{-1} was in good agreement with that of casting pores (61 cm^{-2}) exposed at fracture surface of the specimen deformed at 10^{-3} s^{-1} (Fig. 6b), indicating that the coarser dimples are developed from casting pores.
c) A strong dynamic recovery took place in the test with low strain rate, since the microhardness obtained on the specimen tested at 10^{-6} s^{-1} showed no work hardening, whereas a hardness increase was measured on the specimens tested at higher strain rates (Fig. 8).

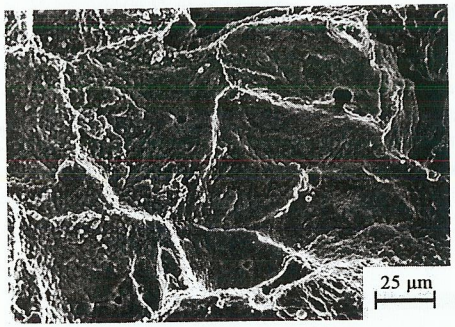

Fig. 7 Casting pores at the bottom of dimples

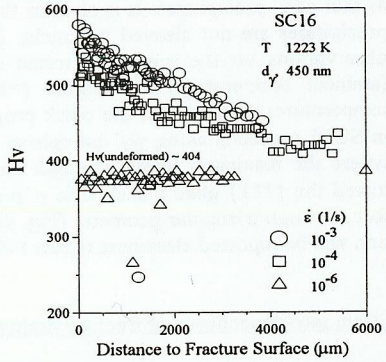

Fig. 8. Microhardness distribution within the gauge length at various strain rates

A mechanism based on the above results is suggested to interpret the observed strain rate-related change in fractographic characteristics and the strain rate-dependence of fracture strain:

In the case of the *high strain rate*, plastic deformation begins at the statistically weakest region, e.g. cross section with a higher local pore density. The material in this region is work hardened due to the plastic deformation, so that the further deformation must transfer into the next weakest region. This process repeated until the whole gauge length of the specimen is work hardened. The specimen is, in this case, homogeneously deformed, fails only if the ductility of the material in the whole gauge length is exhausted and has, therefore, a large fracture strain.
At *low strain rate*, e.g. 10^{-6} s^{-1}, work hardening does not take place due to dynamic recovery. The weakest region where the plastic deformation starts, remains as such or becomes even weaker during the whole deformation process, since the deformation rate in this region is higher than the average one in the gauge length of the specimen, leading to a localised reduction of effective cross section by transverse contraction, casting pore growth or earlier crack nucleation and faster crack propagation. The formation of coarser dimples is caused by link-up of two neighbouring pores or cracks in this locally more damaged region. According to this mechanism a localisation of deformation and damage in the region close to the fracture surface is expected in the case of low strain rate, which leads to an earlier failure and therefore a lower fracture strain. A further evidence is given in Fig. 9. The crack formation and growth in the specimen deformed at high strain rate was quite homogeneous in gauge length of the specimen (Fig. 9a), whereas at low strain rate both the processes took place merely in the region close to the fracture surface (Fig. 9b).

SUMMARY AND CONCLUSIONS

- The crack initiation sites in SC16 have been found to be casting pores.
- The crack preferred to grow along the γ/γ' interphase interfaces, except in the intermediate temperature region (923 K), where the crack propagation occurred on {111} glide plane.
- At high temperature of 1223 K a strain rate-dependence of fracture strain and a corresponding change in fractographic morphology at fracture surfaces were observed. This effect can be rationalised by a proposed mechanism based on the difference in dynamic recovery behaviour of the specimens tested at different strain rates.

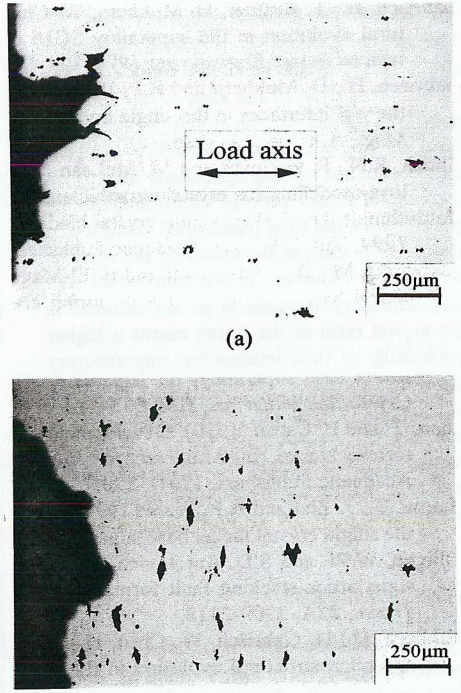

Fig. 9 Cracks in longitudinal sections at a strain rate of 10^{-6} s^{-1} (a) and 10^{-6} s^{-1} (b)

ACKNOWLEDGEMENT

The financial support of Deutsche Forschungsgemeinschaft (DFG) is gratefully acknowledged. The authors would like to thank Mrs. E. Frommbach, H. Malks and Mr. C. Seiler for their technical assistance.

REFERENCES

Ai, D.N., V. Lupinc and M. Maldini (1992). Creep fracture mechanisms in single crystal superalloys, *Scr. metall. mater.*, **26**, 579-584.
Chen, W., M. Rumi, H. Fecht and R.P. Wahi (1996). Mechanical behaviour of single crystal superalloy SC16 under monotonic loading, *Z. Metallkde,* to be published.
Duhl, D.N. (1988). In: Superalloys, Supercomposites and Superceramics, Academic Press (1989), 150.
Fritzemeier, L.G. (1988). The influence of high thermal gradient casting, hot isostatic pressing and alternate heat treatment on the structure and properties of a single crystal nickel base superalloy, In: *Superalloys 1988*, The Metallurgical Soc., 265-274.

Gabrisch, H., T. Kuttner, D. Mukherji, W. Chen, R.P. Wahi and H. Wever (1994). Microstructural evolution in the superalloy SC16 under monotonic loading, In: *Materials for Advanced Power Engineering 1994*, Vol. II, Kluwer Academic Publishers, 1119-1124.

Gabrisch, H., D. Mukherji and R.P. Wahi (1996). Deformation induced dislocation networks at the γ/γ' interfaces in the single crystal superalloy SC16: a mechanism based analysis, *Phil. Mag.*, **A**, to be published.

Ghosh, R.N., R.V. Curtis and M. McLean (1990). Creep deformation of single crystal superalloys-modelling the crystallographic anisotropy, *Acta metall. mater.*, **38**, 1977-1992.

Goldschmidt, D. (1994). Single crystal blades, In: *Materials for Advanced Power Engineering 1994*, Vol. I, Kluwer Academic Publishers, 661-674.

Hashem, A.M., D. Goldschmidt and E. El-Magd (1994). Cavitation damage of the single crystal nickel base superalloy SRR99 during creep at 580°C, *Mat.-wiss. u. Werkstofftech.*, **25**, 133-138.

Kakehi, K., T. Sakaki and T. Adachi (1993). Creep and fatigue strength of single crystals of a nickel base superalloy, In: *Aspects of High Temperature Deformation and Fracture in Crystalline Materials*, JIM, 535-542.

Khan, T. and P. Caron (1990). Development of a new single crystal superalloy for industrial gas turbine blades, In: *Materials for Advanced Power Engineering 1990*, Vol. II, Kluwer Academic Publishers, 1261-1270.

Malow, T., J. Zhu and R.P. Wahi (1994). Influence of heat treatment on the microstructure of the single crystal nickel base superalloy SC16, *Z. Metallkde.*, **85**, 9-19.

Milligan, W.W. and S.D. Antolovich (1991). The mechanisms and temperature dependence of superlattice stacking fault formation in the single crystal superalloy PWA 1480, *Metall. Trans.*, **22A**, 2309-2318.

Mukherji, D., H. Gabrisch, W. Chen, H.-J. Fecht and R.P. Wahi (1996). Softening behaviour and microstructural evolution in the single crystal superalloy SC16, *Acta metall. mater.*, to be published.

Pollock, T.M. and A.S. Argon (1992). Creep resistance of CMSX-3 nickel base superalloy single crystals, *Acta metall. mater.*, **40**, 1-30.

Rumi, M., W. Chen, D. Mukherji, T. Kuttner, R.P. Wahi and H. Wever (1994). Influence of strain rate on the fracture behaviour of the single crystal superalloy SC16 under tensile loading, In: *Materials for Advanced Power Engineering 1994*, Vol. II, Kluwer Academic Publishers, 1165-1174.

Socrate, S. and D.M. Park (1993). Numerical determination of the elastic driving force for directional coarsening in Ni superalloys, *Acta metall. mater.*, **41**, 2185-2209.

Walston, W.S., I.M. Bernstein and A.W. Thompson (1991). The role of the γ/γ' eutectic and porosity on the tensile behaviour of a single crystal nickel base superalloy, *Metall. Trans.*, **22A**, 1443-1451.